Glacial-interglacial dynamics of the eastern equatorial Pacific cold tongue-Intertropical Convergence Zone system reconstructed from oxygen isotope records

Athanasios Koutavas[1] and Jean Lynch-Stieglitz
Lamont-Doherty Earth Observatory, Columbia University, Palisades, New York, USA

Received 19 February 2003; revised 24 May 2003; accepted 15 August 2003; published 4 December 2003.

[1] We use planktonic oxygen isotope ($\delta^{18}O$) records spanning the last 30,000 years (kyr) to constrain the magnitude and spatial pattern of glacial cooling in the upwelling environment of the eastern equatorial Pacific (EEP). Fourteen new downcore $\delta^{18}O$ records were obtained from surface-dwelling planktonic foraminifera *Globigerinoides sacculifer* and *Globigerinoides ruber* in eight cores from the upwelling tongue of the EEP. All sites have sedimentation rates exceeding 5 cm/kyr and, with one exception, lie above the modern depth of the foraminiferal lysocline. Sites directly underlying the cool band of upwelling immediately south of the equator record mean late Holocene (LH)-Last Glacial Maximum (LGM) $\delta^{18}O$ amplitudes ranging between 1.0 and 1.3‰. We estimate that mean sea surface temperatures (SST) in this region during the LGM were on average 1.5 ± 0.5°C lower than the LH. Larger $\delta^{18}O$ amplitudes are observed in sites north of the equator, indicating a spatial pattern of reduced meridional SST gradient across the equator during the LGM. This result is supported by comparison of Mg/Ca SST reconstructions from two sites straddling the equator. We interpret the reduction of this gradient during the LGM as evidence for a less intense cold tongue-Intertropical Convergence Zone (ITCZ) frontal system, a more southerly position of the ITCZ, and weaker southeast equatorial trades in the EEP. *INDEX TERMS:* 1620 Global Change: Climate dynamics (3309); 3339 Meteorology and Atmospheric Dynamics: Ocean/atmosphere interactions (0312, 4504); 3344 Meteorology and Atmospheric Dynamics: Paleoclimatology; 4231 Oceanography: General: Equatorial oceanography; 4267 Oceanography: General: Paleoceanography; *KEYWORDS:* cold tongue, ITCZ, oxygen isotopes, tropical Pacific

Citation: Koutavas, A., and J. Lynch-Stieglitz, Glacial-interglacial dynamics of the eastern equatorial Pacific cold tongue-Intertropical Convergence Zone system reconstructed from oxygen isotope records, *Paleoceanography*, *18*(4), 1089, doi:10.1029/2003PA000894, 2003.

1. Introduction

[2] Tropical SSTs influence atmospheric heating and circulation patterns across much of the globe. Interannual- and decadal-scale SST variations in the tropical Pacific are correlated with global temperature and rainfall anomalies [*Halpert and Ropelewski*, 1992; *Trenberth et al.*, 1998] and impact Earth's radiative balance [*Soden*, 1997; *Pierrehumbert*, 2000] and carbon cycle [*Murray et al.*, 1994, *Chavez et al.*, 1999]. Long-term, orbitally forced variations in tropical Pacific temperatures have been recently studied in models, indicating a key role for precession in controlling mean SST structure through its influence on the seasonal cycle and the El Niño-Southern Oscillation (ENSO) [*Clement et al.*, 1999; *Clement and Cane*, 1999; *Cane and Clement*, 1999; *Codron*, 2001]. Because of its potential for interhemispheric teleconnections and perturbations of the global radiation balance through CO_2, water vapor and cloud mechanisms, the tropical Pacific ocean-atmosphere system may play a key role in synchronizing climate shifts between the hemispheres [*Cane*, 1998; *Cane and Clement*, 1999]. To fully understand the role of this system in glacial-interglacial transitions, an accurate knowledge of the amplitude, timing and spatial fingerprint of SST variations in this region is required. In this study we are primarily concerned with oceanographic changes in the EEP during the last deglaciation and their implications for the evolution of the regional cold tongue-ITCZ frontal complex, the latter being a key diagnostic for upwelling and atmospheric convection in the EEP [*Mitchell and Wallace*, 1992; *Deser and Wallace*, 1990], and hence intricately linked to ENSO processes.

2. Background

[3] The Climate: Long-Range Investigation, Mapping, and Prediction (CLIMAP) project produced the first estimate of the global SST field during the LGM using faunal assemblage techniques [*CLIMAP Project Members*, 1981]. Averaged over the tropical Pacific, reconstructed winter (Feb) and summer (Aug) SST anomalies were minimal (~1°C) and their pattern suggested reduced zonal and meridional SST gradients. CLIMAP results in the tropics have been questioned, as they are in apparent conflict with terrestrial records suggesting substantially larger tropical cooling [*Rind and Peteet*, 1985] (see also review by

[1]Now at Department of Earth, Atmospheric and Planetary Sciences, Massachusetts Institute of Technology, Cambridge, Massachusetts, USA.

0883-8305/03/2003PA000894$12.00

Crowley [2000]). Further, general circulation models (GCMs) have been unable to cool land surfaces sufficiently when CLIMAP LGM SSTs are prescribed. In the EEP where faunal methods are complicated by the no-analog problem [*Mix et al.*, 1999] and dissolution concerns are exacerbated by high productivity and elevated organic carbon in sediments, CLIMAP results are deemed least reliable.

[4] A long-standing paradigm that has endured for nearly two decades calls for intensified upwelling in the EEP during glacial periods as an explanation for increased productivity, inferred from sedimentary organic carbon [*Pedersen*, 1983; *Lyle et al.*, 1988; *Pedersen et al.*, 1991] and barite [*Paytan et al.*, 1996] accumulation rates. The postulated increase in upwelling is commonly attributed to strengthened equatorial trade winds, such as occur in some GCM simulations of the LGM climate [e.g., *Bush and Philander*, 1999]. Nevertheless, the link between productivity and upwelling is indirect, particularly in high-nutrient low-chlorophyll regions such as the EEP where primary production is limited by iron [*Coale et al.*, 1996] and may be further regulated by silicate availability [*Dugdale and Wilkerson*, 1998]. Moreover, at least one study indicates reduced productivity in this region during the LGM [*Loubere*, 2000], and some of the evidence for increased productivity may be an artifact of sediment focusing [*Marcantonio et al.*, 2001]. Decoupling of SST from organic flux variations in a central equatorial Pacific site led *Lyle et al.* [1992] to suggest that horizontal advection of cooler surface waters from high latitudes rather than upwelling was the likely cause of glacial cooling. Studies utilizing interspecies foraminiferal $\delta^{18}O$ and $\delta^{13}C$ differences in ODP sites 847 [*Farrell et al.*, 1995] and 851 [*Ravelo and Shackleton*, 1995] are consistent with reduced glacial SSTs by 1°–3°C, but their interpretations differ as to whether upwelling or advection was the dominant cooling agent. A more recent reconstruction by *Faul et al.* [2000] similarly found no clear evidence for enhanced glacial upwelling rates. Meanwhile, thermocline depth estimates based on transfer functions [*Andreasen and Ravelo*, 1997] have indicated a steeper east-west thermocline tilt during the LGM, with shoaling in the east-central and deepening in the western equatorial Pacific. A follow-up modeling study attributed this pattern to strengthened winds primarily in the western Pacific resulting from LGM boundary conditions [*Andreasen et al.*, 2001].

[5] Recent studies using recalibrated radiolarian and foraminiferal transfer functions have suggested that LGM temperatures may have been up to 5°C colder than present in a concentrated area of the equatorial cold tongue, with decreasing anomalies away from the equator [*Pisias and Mix*, 1997; *Mix et al.*, 1999; *Feldberg and Mix*, 2002, 2003], a pattern suggestive of enhanced equatorial divergence. Recent application of the modern analogue technique (MAT) is in qualitative agreement with these cooling estimates [*Trend-Staid and Prell*, 2002; *Martínez et al.*, 2003] and in some cases exceeds them. Using Mg/Ca paleothermometry, *Lea et al.* [2000] estimated that glacial SSTs were lower by 2.5°–3.0°C in a set of cores on the Cocos Ridge just north of the equator, similar or marginally higher than their estimate for a western Pacific site on the Ontong-Java Plateau. Using coccolithophorid abundances as productivity indicators *Beaufort et al.* [2001] inferred ENSO-like hydrographic variability at precessional frequencies, and interpreted it in terms of a dynamical response akin to La Niña conditions during glacials, although this mode of variation explained only a minor (∼20%) part of their records. By contrast, on the basis of minimal LGM cooling of 1°–1.5°C near the center of the cold tongue reconstructed from Mg/Ca ratios in a site near the Galapagos Islands, *Koutavas et al.* [2002] proposed a mean climate state characterized by reduced SST gradients and zonal winds near the equator. This hypothesis is in agreement with an apparent glacial increase of surface salinity in the Indonesian Archipelago, deduced from paired Mg/Ca-$\delta^{18}O$ measurements in planktonic foraminifera near the southern Philippines and attributed to an eastward shift of the warm pool [*Stott et al.*, 2002]. Thus despite ongoing and concerted efforts to understand fundamental aspects of the oceanographic response of the EEP over glacial-interglacial cycles a consensus has yet to emerge and acute discrepancies among varied methodologies remain. Here we employ an approach based on the $\delta^{18}O$ of spinose planktonic foraminifera and their ability to monitor the prominent equatorial front present in the EEP.

[6] Oxygen isotope ratios in planktonic foraminifera have a long history of use as a surface temperature proxy. Data by *Shackleton* [1977] were used by *Broecker* [1986] to infer near-zero LGM cooling in the tropical Pacific, but these data have been questioned because of low sedimentation rates and possible dissolution artifacts. Because most studies utilizing foraminiferal $\delta^{18}O$ in the EEP have been limited by complications from dissolution, bioturbation, incomplete Holocene sections, low sedimentation rates and poor dating, a clear understanding of the glacial-interglacial pattern of $\delta^{18}O$ variations and its climatic implications in the EEP has yet to emerge. To fill this gap we obtained 14 new downcore $\delta^{18}O$ profiles measured on the mixed-layer species *G. sacculifer* and *G. ruber* from 8 sites in the EEP. Our site selection strategy aimed at sampling primarily the upwelling region near the center of the cold tongue 1°–2° south of the equator, without exceeding the depth of accelerated calcite dissolution of ∼2800 m [*Thunell et al.*, 1981]. Only sites with deposition rates sufficiently high (>5 cm/kyr) were selected to ensure that Holocene and glacial samples were not mixed by bioturbation. ^{14}C dating was carried out in all cores to ensure proper identification of the LGM and LH sections and allow site intercomparison. Sites straddling the equator were compared to obtain a sense of changes in the cross-equatorial gradient from the LGM to the Holocene. Our results are consistent with previous indications of a reduced cross-equatorial front in glacial times [*Koutavas et al.*, 2002] and imply a weaker cold tongue-ITCZ complex. In the following sections we present these results and explore their implications for glacial-interglacial dynamics of the tropical Pacific ocean-atmosphere system.

3. Oceanographic Setting

[7] In the EEP upwelling favorable southeasterly trade winds blow year-round, albeit with seasonal variations,

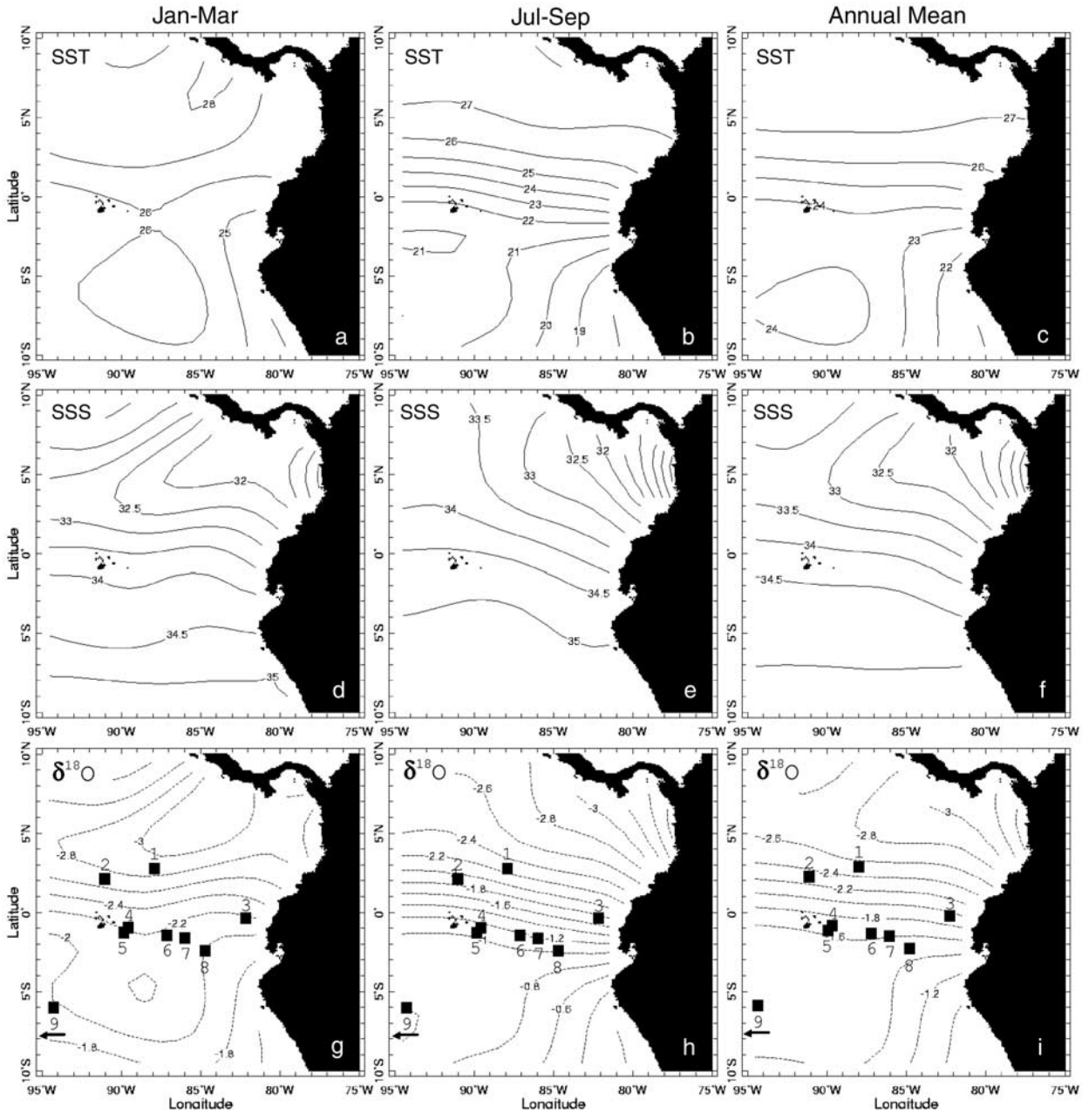

Figure 1. Sea surface temperature (SST) and salinity (SSS) for seasonal extremes and annual mean conditions in the EEP. To first approximation the Jan–Mar seasonal pattern resembles El Niño conditions, while the Jul–Sep pattern resembles La Niña conditions. SST is shown in Figures 1a–1c [*Levitus and Boyer*, 1994], and SSS in Figures 1d–1f [*Levitus et al.*, 1994]. Figures 1g–1i show the corresponding seasonal and annual mean fields in predicted $\delta^{18}O$ of foraminiferal calcite calculated using the low-light paleotemperature equation of *Bemis et al.* [1998] and the seawater $\delta^{18}O$-salinity equation of *Fairbanks et al.* [1982]. Note that the seasonal intensification of the meridional SST gradient from the warm to the upwelling season (Figures 1a and 1b) is clearly reflected in the predicted $\delta^{18}O$ field (Figures 1g and 1h), as is the case for the annual mean gradient (Figures 1c and 1i). By comparison with SST, salinity contributes little to the seasonal intensification of the $\delta^{18}O$ gradient, as the salinity front maintains its strength through the seasons (Figures 1d and 1e). The locations of cores used in the present study are shown in the bottom panels with filled squares, numbered from north to south as follows: 1, RC13-140; 2, TR163-19; 3, V19-27; 4, V21-29; 5, V21-30; 6, RC8-102; 7, RC11-238; 8, V19-28; 9, V21-40. Arrow below site 9 (V21-40) in the southwest corner indicates that this site is in fact positioned further west, at a longitude of 106°46′W. Site coordinates are listed in Table 1.

Table 1. List of Cores Used in This Study[a]

CORE	Latitude	Longitude	Depth, m	Species	LH $\delta^{18}O$, ‰	LGM $\delta^{18}O$, ‰	$\Delta\delta^{18}O$, ‰	ΔT, °C
RC8-102	1°25′S	86°51′W	2180	*G. sacculifer*	−1.23	−0.29	0.94	0.3
				G. ruber	−1.78	−0.45	1.33	−1.6
RC11-238	1°31′S	85°49′W	2573	*G. sacculifer*	−1.29	−0.09	1.20	−1.0
				G. ruber	−1.56	−0.29	1.27	−1.3
RC13-140	2°52′N	87°45′W	2246	*G. sacculifer*	−2.03	−0.50	1.53	−2.5
				G. ruber	−2.66	−0.96	1.70	−3.3
TR163-19	2°15′N	90°57′W	2348	*G. ruber*	−2.19	−0.61	1.58	−2.8
V19-27	0°28′S	82°04′W	1373	*G. sacculifer*	−1.87	−0.35	1.52	−2.5
				G. ruber	−2.14	−0.67	1.47	−2.4
V19-28	2°22′S	84°39′W	2720	*G. sacculifer*	−1.29	−0.21	1.08	−0.4
				G. ruber	−1.57	−0.27	1.30	−1.4
V21-29	1°03′S	89°21′W	712	*G. sacculifer*	−1.45	−0.49	0.96	0.2
V21-30	1°13′S	89°41′W	617	*G. sacculifer*	−1.46	−0.32	1.14	−0.7
				G. ruber	−1.73	–	–	–
V21-40	5°31′S	106°46′W	3182	*G. sacculifer*	−1.24	−0.13	1.11	−0.5
				G. ruber	−1.55	−0.48	1.07	−0.3

[a]Average $\delta^{18}O$ values for the LH and LGM are indicated, as well as their difference ($\Delta\delta^{18}O$) and the implied temperature anomalies (ΔT) estimated as explained in the text. Negative ΔT values indicate cooling during the LGM.

across the equator and into the ITCZ overlying the warm waters of the northeast tropical Pacific warm pool [*Mitchell and Wallace*, 1992; *Li and Philander*, 1996; *Chelton et al.*, 2001]. Upwelling along the equator forms a tongue of cool waters extending westward from the Peruvian coastal upwelling zone to the dateline. The upwelling of cold, salty, nutrient-rich waters establishes strong temperature, salinity, and nutrient gradients northward across the equator [e.g., *Pak and Zaneveld*, 1974]. The frontal zone between the cold tongue and ITCZ features one of the world's steepest tropical SST gradients, with a seasonal maximum exceeding 1°C per degree of latitude (∼100 km) between 0°–5°N (Figure 1).

[8] Seasonal intensification of this front occurs in boreal summer (Jul–Aug–Sep) (Figure 1b) when cold-tongue upwelling is most intense, SSTs are lowest, and the ITCZ is positioned furthest north. During austral summer (Jan–Feb–Mar) the front attenuates, upwelling diminishes, and the ITCZ shifts south (Figure 1a). Despite the dominant semi-annual insolation cycle at the equator (the sun crosses the equator twice a year) the seasonal SST cycle in the EEP has a pronounced annual period, which is forced by the strong equatorial asymmetry in winds, SST and cloud cover, and demonstrates the critical influence of ocean-atmosphere interactions on the mean climatology of this region [*Li and Philander*, 1996].

[9] Interannually, during peak El Niño the frontal system vanishes as the thermocline deepens and reduced upwelling fails to form a cold tongue at the equator. In contrast, La Niña events cause the front to intensify [*Deser and Wallace*, 1990]. Monthly SST anomalies in the cold tongue associated with warm ENSO episodes can reach +5°C, while negative anomalies up to −3°C are observed during cold episodes. Shifts in the position of organized convection in the tropical atmosphere associated with these anomalies impact the global circulation, setting off teleconnections via Rossby wave propagation from the tropics to midlatitudes [*Trenberth et al.*, 1998]. Teleconnections are observed on decadal timescales as well, as for instance during the climate shift of 1976 [*Trenberth and Hurrell*, 1994]. Furthermore, century-scale links between tropical Pacific temperature/salinity variations and global climate have been inferred from coral proxy reconstructions [*Hendy et al.*, 2002; *Urban et al.*, 2000].

[10] In light of the recent interannual and decadal observations of ENSO and associated tropical-extratropical interactions, the notion that shifts in tropical SST patterns may be important for glacial-interglacial climate variations as well, is not surprising. It is supported by at least one modeling study [*Yin and Battisti*, 2001] which concluded that the altered SST gradients implicit in the CLIMAP reconstruction are at least as important for the midlatitude circulation as a uniform cooling of the tropics by 3°C. Thus estimates of mean tropical cooling alone no longer appear sufficient for understanding essential LGM climate features; a sense of the spatial heterogeneity in LGM SST anomalies is required as well. To this end our study attempts a reconstruction of the glacial-interglacial pattern of variation in the cross-equatorial oceanographic front of the eastern tropical Pacific, by many measures a sensitive and essential diagnostic of coupled ocean-atmosphere dynamics across the entire Pacific basin.

4. Materials and Methods

[11] We obtained 14 downcore $\delta^{18}O$ profiles on *G. sacculifer* (without final sac) and *G. ruber* (white) in eight cores from the EEP (Table 1 and Figure 1). Five of these cores (V21-29, V21-30, RC8-102, RC11-238, V19-28) lie in a narrow belt between 1°–2.5°S and 84°–90°W along the Carnegie Ridge, directly underlying the equatorial upwelling tongue east of the Galapagos Islands. Another core (V21-40) is located further southwest, in the path of the South Equatorial Current. The easternmost site (V19-27) is located closest to shore, ∼150 km off the coast of Ecuador. The region north of the equator is represented by RC13-140 located on the Cocos ridge, and is supplemented by the $\delta^{18}O$ record of *G. ruber* from nearby core TR163-19, obtained by *Lea et al.* [2000].

[12] We measured $\delta^{18}O$ on ∼12 and ∼15 shells of *G. sacculifer* and *G. ruber* per sample, respectively.

Table 2. Radiocarbon Ages Used to Construct the Age Models of the Cores Used in This Study[a]

CORE	Depth, cm	^{14}C Age, Years	Age Error, ± Years	Calibrated Age, Years	1-σ Range, Years	NOSAMS Accession Number
RC8-102	0	5150	30	5385	5568–5326	OS-33383
	49	14000	55	16270	16508–16046	OS-33384
	101	20100	65	23290	23690–22922	OS-33385
RC11-238	0	3570	60	3360	3385–3267	–
	40	8210	50	8530	8592–8433	–
	80	14180	70	16480	16725–16244	–
	100	17100	60	19840	20162–19527	–
RC13-140	0	1750	25	1260	1276–1183	OS-33386
	50	10450	45	11440	11553–11260	OS-33387
	100	16850	55	19550	19870–19245	OS-33388
	151	24300	85	26690	–	OS-33389
V19-27	0	1340	25	790	884–742	OS-33390
	49	5710	30	5990	6167–5945	OS-33391
	90	14200	65	16500	16746–16268	OS-33422
	150	26300	140	29840	–	OS-33423
V19-28	6	2240	30	1710	1731–1631	OS-33424
	53.5	9510	40	10220	10236–10192	OS-33425
	101	12750	50	14290	15285–14131	OS-33426
	146	16100	60	18690	18993–18404	OS-33427
	193.5	27000	120	31270	–	OS-33428
V21-29	0	1600	35	1060	1166–989	OS-33429
	101	13400	50	15575	15798–15191	OS-33533
	148	14950	55	17365	17627–17118	OS-33534
V21-30	0	2190	45	1660	1709–1569	OS-20675
	55	5620	55	5920	5987–5906	OS-30482
	120	9830	55	10620	10687–10506	OS-20674
	151	11250	50	12890	12960–12659	OS-20676
	161*	13400	75	–	–	OS-21890
	170	11750	90	13180	13429–13148	OS-30483
	184	12250	70	13820	14004–13609	OS-30484
	215	13400	90	15580	15816–15175	OS-30485
	250	16800	80	19490	19818–19182	OS-20680
	320	25100	150	27360	–	OS-30486
	400	26900	150	31160	–	OS-15720
V21-40	0	2700	30	2250	2334–2161	OS-33535
	50	10000	45	11200	11084–10699	OS-33536
	78	16250	60	18860	19169–18571	OS-33537
	120	25700	110	27940	–	OS-33538

[a]Raw ages were corrected by −450 years for reservoir effect and calibrated with the use of the Calib 4.3 software [*Stuiver et al.*, 1998]. The 1-σ range of the calibrated ages is indicated. With the exception of the previously published ages of RC11-238 [*Faul et al.*, 2000], all ages were measured at the National Ocean Sciences Accelerator Mass Spectrometry (NOSAMS) facility of the Woods Hole Oceanographic Institution, and their accession numbers are listed. All measurements were made on monospecific foraminiferal samples comprised of *N. dutertrei* shells, except the 400 cm sample from core V21-30 where a mix of *N. dutertrei* and *O. universa* was used. Asterisk indicates age rejected as anomalously old.

G. sacculifer was picked from the 355–425 μm size fraction, and *G. ruber* from the 300–355 μm size fraction. Prior to analysis samples were cleaned by sonic agitation in a bath of deionized water. Analyses were made with a Micromass Optima isotope ratio mass spectrometer equipped with Multiprep carbonate preparation device. Instrument calibration is made through routine analysis of NBS-18, NBS-19 and an internal standard. Results are reported with respect to the Vienna Pee Dee Belemnite (VPDB) reference standard. Analytical precision for $\delta^{18}O$ is better than ±0.07‰ (1-σ).

[13] When picking shells care was taken to exclude individuals with visible signs of dissolution such as broken or missing chambers and/or fragile shells. While Holocene-age samples from the deepest cores (>2000 m) contained shells bearing visible signs of dissolution, well-preserved shells were typically present as well, and it was the latter that were selected for analysis. To verify that this practice was effective in minimizing a possible dissolution bias we recorded the mean shell weight of *G. sacculifer* in samples from the deepest core (V21-40, 3182 m) prior to analysis. Mean shell weight is expected to decrease with increasing dissolution due to thinning of chamber walls, while shell size remains unaffected [*Lohmann*, 1995]. Results indicate lack of a glacial-interglacial trend in mean shell weight, which suggests the absence of significant dissolution bias in the analyzed samples.

[14] Age control in all cores is through accelerator mass spectrometry (AMS) ^{14}C dating of foraminifera. AMS-^{14}C analyses were made on monospecific samples comprised of ~200–400 shells of *Neogloboquadrina dutertrei* picked from the >250 μm size fraction. Ages were corrected for reservoir effect by subtracting 450 years from the measured age, and calibrated to calendar years using the INTCAL98 data set [*Stuiver et al.*, 1998]. Ages exceeding the INTCAL98 calibration limit of 24 kyr before present (BP) were calibrated by comparison with the varved chronology of Lake Suigetsu, Japan [*Kitagawa and van der Plicht*, 1998]. AMS-^{14}C dates obtained for this study and their calibrated ages are listed in Table 2. The age model for all

cores is based on linear interpolation/extrapolation of calibrated ^{14}C ages.

5. Oxygen Isotope Results

5.1. Ecologic Habits of *G. Sacculifer* and *G. Ruber*

[15] *G. sacculifer* and *G. ruber* are the most prolific planktonic foraminifera in warm tropical waters. Possession of photosynthetic symbionts by both species leads to life cycles predominantly confined to the upper photic zone [*Bé et al.*, 1982; *Fairbanks et al.*, 1982]. However, both species can add shell mass in cooler waters near the thermocline during gametogenesis at the terminal life stage. The percentage of gametogenic calcite or "crust" added by *G. sacculifer* is estimated at ~28% [*Bé*, 1980; *Lohmann*, 1995; *Rosenthal et al.*, 2000] and considerably less for *G. ruber*. Either species is believed to tolerate temperatures in the range 14°–32°C [*Bijma et al.*, 1990]. *G. sacculifer* has a preferred salinity range of 34.5–36 ‰, while *G. ruber* has a preference for slightly higher or lower salinities [*Bé and Tolderlund*, 1971]. Both species are therefore well suited to the range of hydrographic conditions encountered in the EEP (Figure 1).

[16] Seasonal variations in the flux of these species to the seafloor have been studied in sediment traps from the nearby Panama Basin at 5°N, 82°W [*Thunell et al.*, 1983; *Thunell and Reynolds*, 1984]. In that setting both species exhibited peak fluxes during the warm summer months (Jun–Sep) and secondary peaks during the cool upwelling season (Dec–Mar). The flux-weighted $\delta^{18}O$ composition of sediment trap samples was found to be in agreement with annual mean hydrography over the deployment period [*Curry et al.*, 1983], suggesting the lack of a seasonal bias in $\delta^{18}O$ from seafloor samples. Nevertheless, observations made in the Panama Basin are not readily applicable to the cold-tongue environment where the hydrography is markedly different. In the warmer, more stratified waters of the Panama basin the hydrography is mainly controlled by ITCZ-induced rainfall, which primarily affects surface salinity. By comparison, in the cold tongue the more sensitive hydrographic property is SST, responding to the seasonal intensification of wind-driven upwelling. As a consequence the seasonal cycle is dominated by salinity variations in the Panama Basin, compared to SST variations in the cold tongue. Thus the pattern of seasonal and interannual foraminiferal flux variations in the latter region remains unknown and requires further investigation.

[17] In this study we assume that sediment samples from the studied cores integrate the annual cycle of temperature and salinity over each site, giving a representative view of mean hydrographic conditions over a depositional period of 100–200 years per sample (based on average sample thickness of 1 cm). We further assume that possible seasonal biases in the vertical flux of these species to the seafloor, if present, have remained relatively constant through time. If this assumption were violated in the past it could introduce time-varying seasonal biases in the downcore records which might lead to misrepresentations of the long-term annual mean climate progression. One issue of special concern is whether the temperature tolerance of *G. ruber* and *G. sacculifer* were wide enough to average the annual cycle during the LCM, or whether ocean cooling might instead have limited their growth to the summer season. Assuming a culture-derived lower temperature limit of 14°C for these species [*Bijma et al.*, 1990], we estimate it would require a mean ocean cooling of 6°C at the position of the coldest site today (V19-28, annual mean SST of 23°C) for SST to drop below this limit during the coldest months of the year (using a modern value of 6°C for the amplitude of the annual cycle). Furthermore, such seasonal adjustment in the growth patterns of these species might be expected to introduce a modern warm-season bias in the coldest EEP sites near 1°–2°S, which is not evident in the core-top or Holocene $\delta^{18}O$ data (Figures 2 and 3). The continuous presence of these species throughout the glacial horizons of cores from even the coldest present-day EEP waters [e.g., *Patrick and Thunell*, 1997] suggests that glacial hydrographic changes were not severe enough to eliminate these species from the regional plankton fauna. From these observations we conclude that even though the possibility of seasonal biases cannot be ruled out and merits further study, it does not appear to pose a fundamental restriction on the use of these species for reconstructing glacial-interglacial hydrographic variations in the EEP.

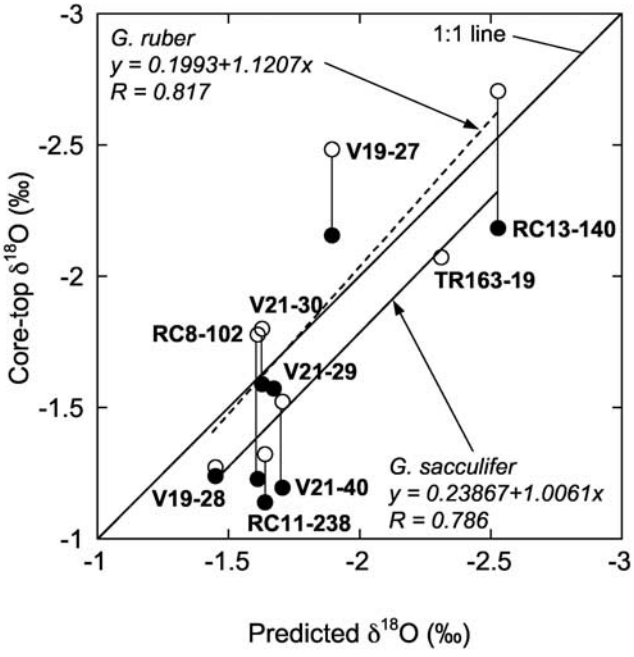

Figure 2. Core-top versus predicted $\delta^{18}O$ of *G. sacculifer* (filled circles) and *G. ruber* (open circles) from the EEP cores used in this study. Linear fits to the data from each species are indicated. The slope of the regressions are close to the 1:1 relationship and suggest that both species respond to the regional hydrography with a sensitivity close to that predicted from equilibrium calcification. Vertical lines connect data from the same core. Possible reasons for the scatter in the data may include noncontemporaneous core-top ages, variable sediment dissolution rates, and variable seasonal/interannual foraminiferal flux biases across sites.

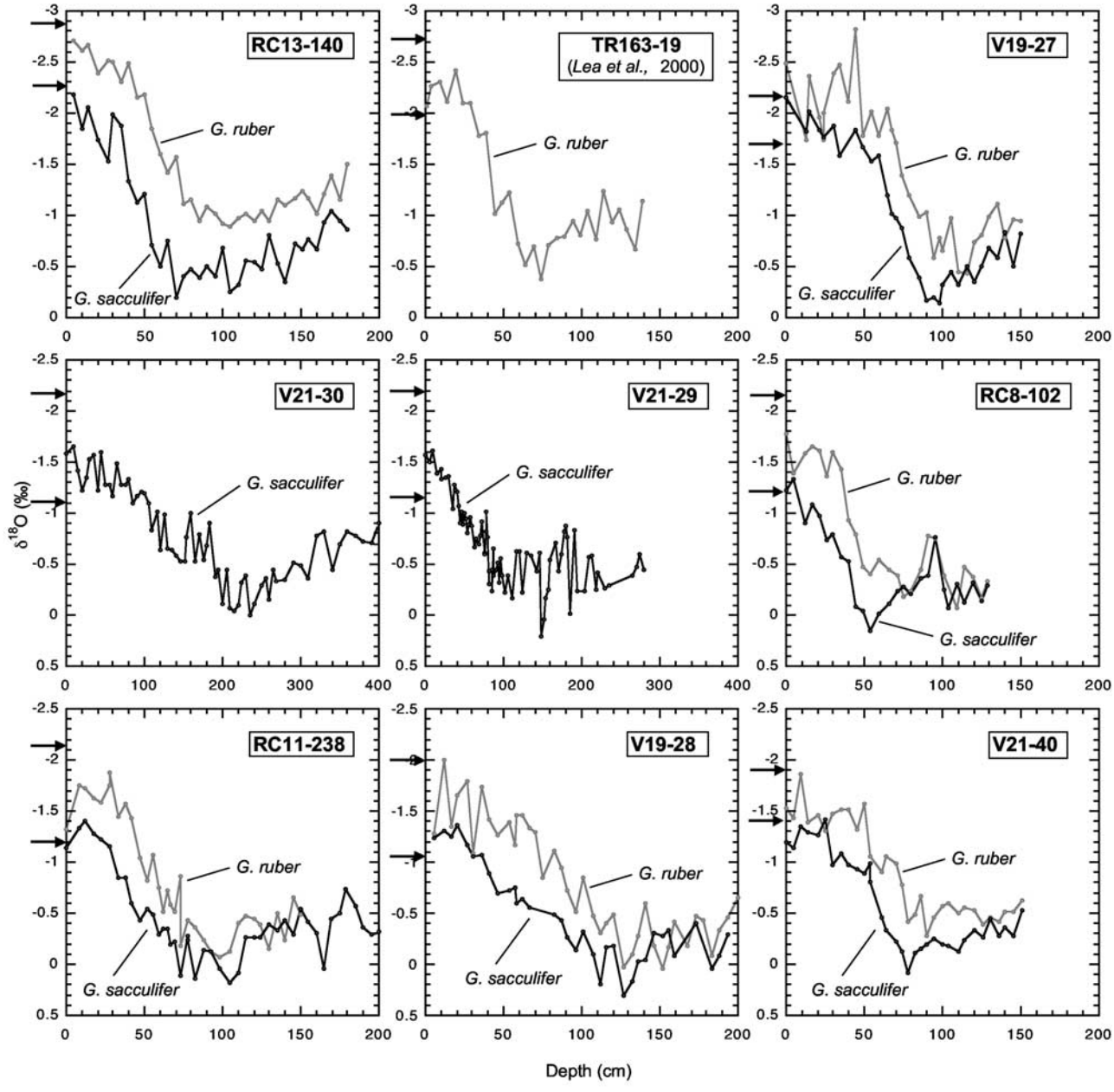

Figure 3. Downcore $\delta^{18}O$-depth profiles measured on *G. sacculifer* and *G. ruber* in the nine EEP sites used in this study. *G. ruber* data from TR163-19 are from *Lea et al.* [2000]. Arrows on the $\delta^{18}O$ axes indicate the seasonal range of predicted $\delta^{18}O$ values for each site as in Figures 1g and 1h.

[18] In Figure 2 core-top $\delta^{18}O$ values from nine EEP sites are plotted versus predicted $\delta^{18}O$ of calcite calculated from annual mean SST and SSS [*Levitus and Boyer*, 1994] using the low-light temperature equation of *Bemis et al.* [1998] and the regional seawater $\delta^{18}O$-salinity relationship of *Fairbanks et al.* [1982]. In general *G. ruber* $\delta^{18}O$ is close to predicted values while *G. sacculifer* $\delta^{18}O$ is slightly heavier. The isotopic offset between the two species is similar to that observed in sediment trap [*Curry et al.*, 1983] and plankton tow samples [*Fairbanks et al.*, 1982], and may be explained by the greater addition of gametogenic calcite by *G. sacculifer* below the surface. Regression of core-top versus predicted $\delta^{18}O$ values for each species gives slopes of 1.0 for *G. sacculifer* and 1.12 for *G. ruber*, close to the 1:1 line.

5.2. Downcore Data

[19] Downcore $\delta^{18}O$ profiles versus depth are shown in Figure 3. In all sites where paired *G. ruber*-*G. sacculifer* data are available, *G. ruber* consistently displays lighter values, although the interspecies isotopic difference is not constant across sites or through time. In order to estimate the magnitude of surface cooling during the LGM we calculated the mean LGM-LH $\delta^{18}O$ difference in the

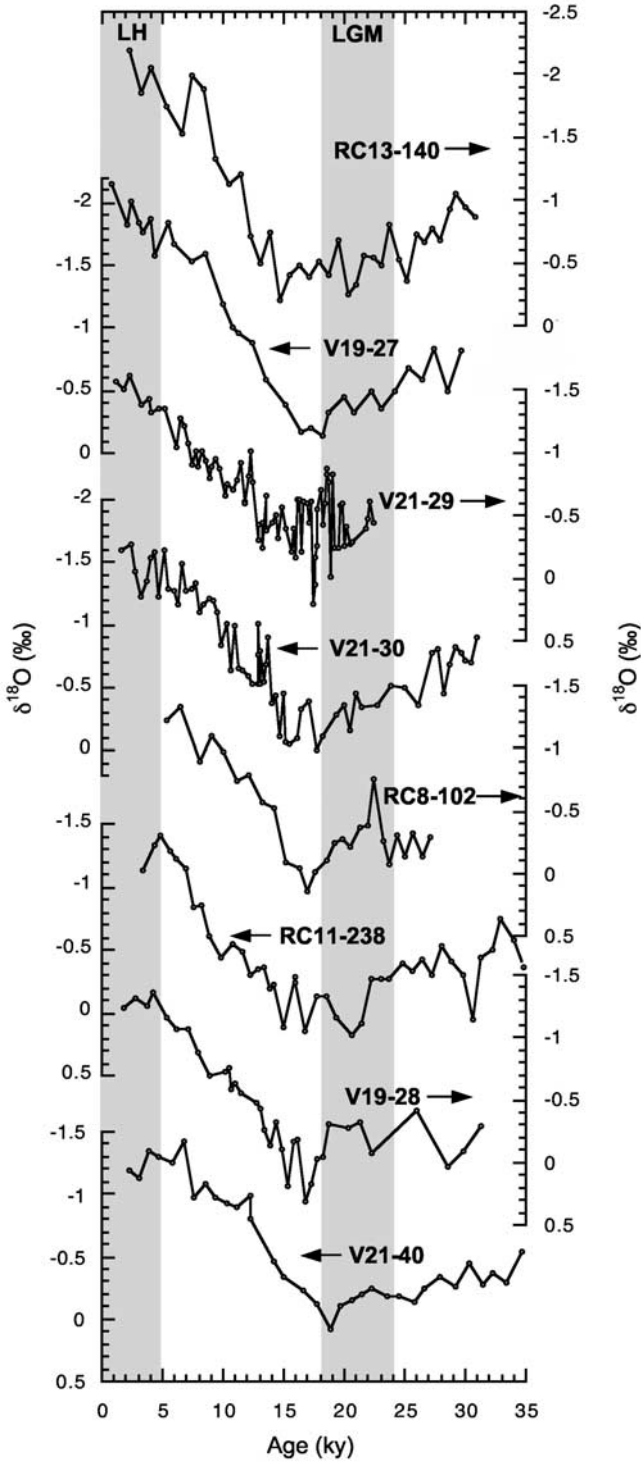

Figure 4. *G. sacculifer* $\delta^{18}O$ profiles from all EEP cores versus age. Arrows next to core names point to respective $\delta^{18}O$ scales. The LGM and LH intervals are shaded.

15 downcore profiles plotted versus calendar age in Figures 4 and 5, for *G. sacculifer* and *G. ruber*, respectively. In all cases our selection of the LGM relied on identification of the 18–24 kyr BP interval by ^{14}C dating as recommended by EPILOG [*Mix et al.*, 2001]. In the case of the Holocene there is growing evidence for regional SST variations [*Koutavas et al.*, 2002; *Andrus et al.*, 2002; *Liu et al.*, 2003] although their sense, magnitude and regional pattern are debated. To minimize a bias due to inclusion of early to middle Holocene data possibly representing cooler (or warmer) surface temperatures we selected the LH as

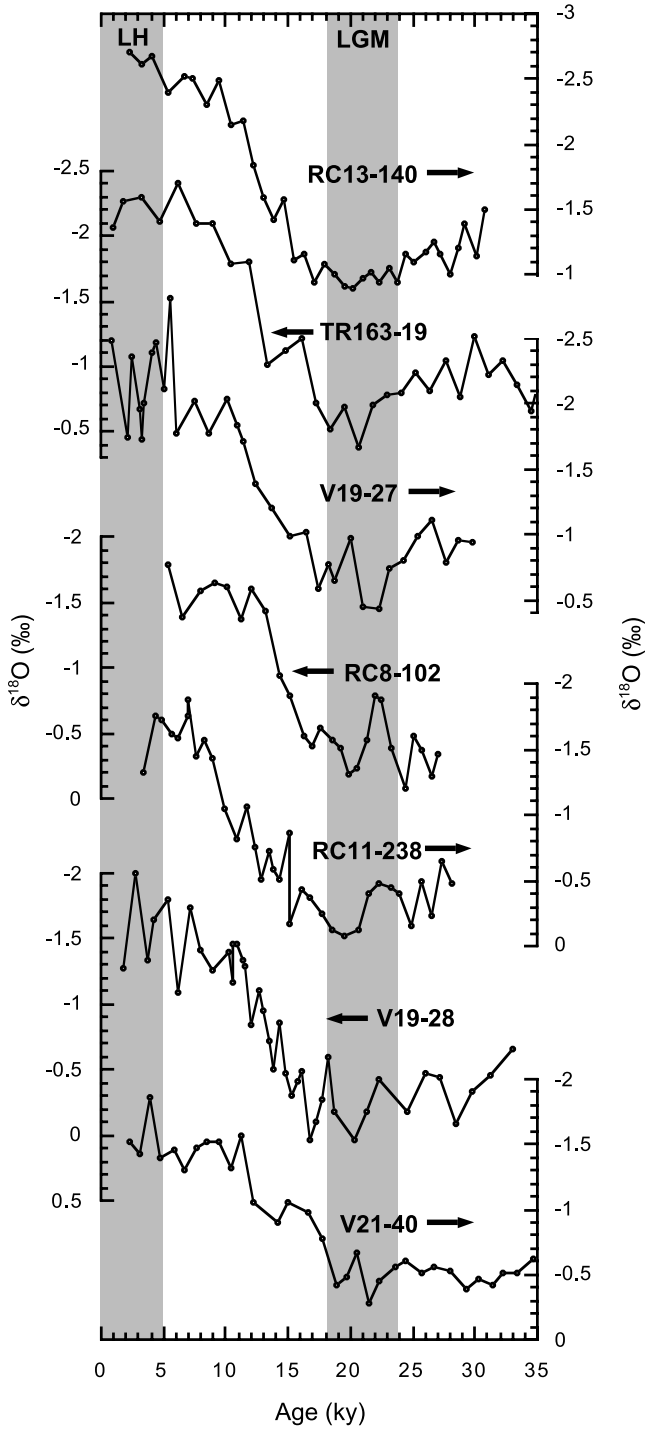

Figure 5. As in Figure 4 but for *G. ruber*.

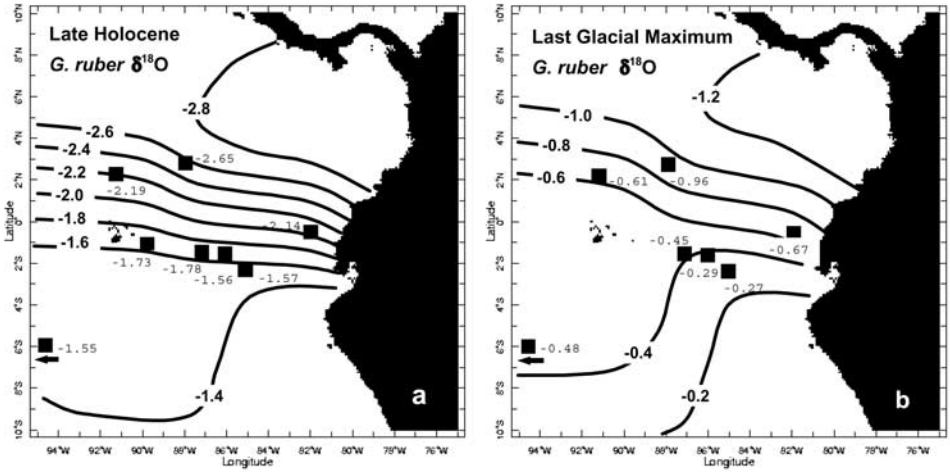

Figure 6. Map view of *G. ruber* $\delta^{18}O$ values averaged over the LH and LGM intervals of 8 EEP cores. Contours reflect our proposed structure of the foraminiferal calcite $\delta^{18}O$ field, indicative of mean (a) LH and (b) LGM hydrographic conditions. For comparison, the modern $\delta^{18}O$ field calculated from hydrographic data is shown in Figure 1i. We interpret the reduced strength of the LGM $\delta^{18}O$ gradient as evidence for a weaker equatorial cold tongue associated with a southward shift of the ITCZ.

the interval between 0 and 5 kyr BP. In most cases 3–9 measurements were averaged to obtain a mean LH and LGM $\delta^{18}O$ value. (One exception is core RC8-102 whose LH section is missing; we used core-top $\delta^{18}O$ values from this core, dated to 5385 y BP, as indicative of the LH.) In Figure 6 average LH and LGM $\delta^{18}O$ values of *G. ruber* from 8 sites were used to map the regional calcite $\delta^{18}O$ field during these two time slices. Mean LGM-LH $\delta^{18}O$ differences ($\Delta\delta^{18}O_{LGM\text{-}LH}$) from both *G. ruber* and *G. sacculifer* are mapped in Figure 7a. Observed amplitudes range between

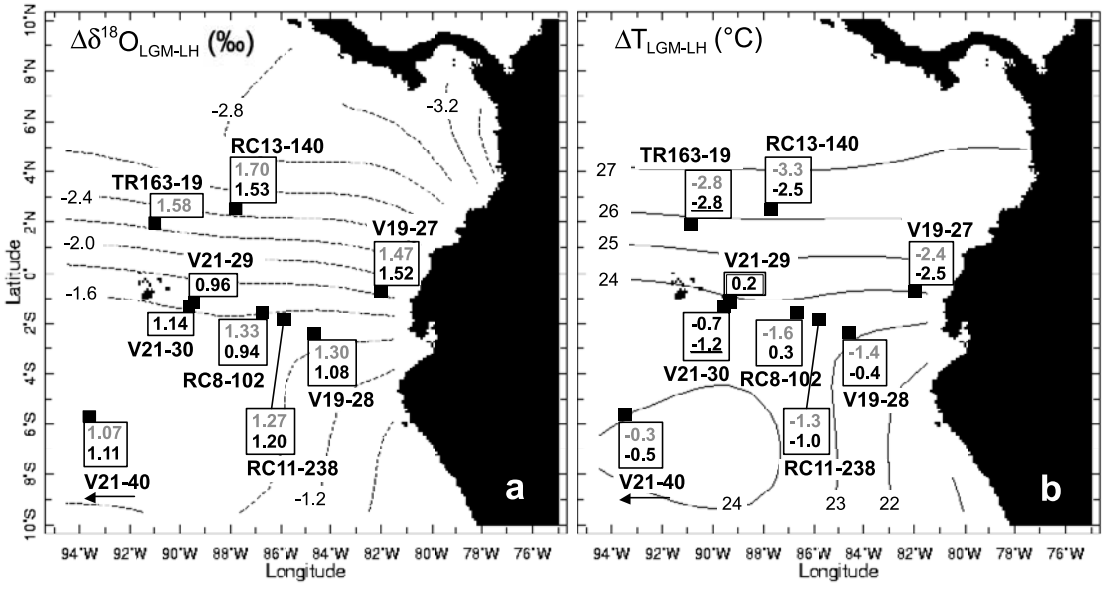

Figure 7. Map view of mean LGM-LH anomalies in $\delta^{18}O$ and temperature, reconstructed from the studied EEP sites. (a) Mean LGM-LH $\delta^{18}O$ amplitudes ($\Delta\delta^{18}O_{LGM\text{-}LH}$) measured on *G. ruber* (numbers in grey), and *G. sacculifer* (numbers in black). The background contours indicate predicted calcite $\delta^{18}O$ values based on modern annual mean SST and SSS, as in Figure 1i. (b) LGM-LH temperature anomalies ($\Delta T_{LGM\text{-}LH}$) calculated from the $\Delta\delta^{18}O_{LGM\text{-}LH}$ values shown in Figure 7a, as discussed in the text. Estimates from *G. ruber* $\delta^{18}O$ are in grey, from *G. sacculifer* $\delta^{18}O$ are in black, and from Mg/Ca in TR163-19 [*Lea et al.*, 2000] and V21-30 [*Koutavas et al.*, 2002] are underlined. Negative ΔT values indicate cooling during the LGM. The background contours show the modern annual mean SST structure. As in Figure 1, the arrows under site V21-40 indicate its actual position is further west, at 106°46′W.

~1.0–1.7 ‰. Highest $\Delta\delta^{18}O_{LGM-LH}$ values are found in the 3 northernmost sites (1.5–1.7‰) and lowest in the 6 southern sites (1.0–1.3‰). The most direct implication of these data is a reduced LGM meridional $\delta^{18}O$ gradient (Figure 6) that reflects the gradients in temperature and salinity. This result is discussed in detail in subsequent sections.

5.3. LGM Temperature Anomalies

[20] To convert $\delta^{18}O$ amplitudes to SST anomalies we first applied a correction of 1‰ to account for the mean ^{18}O enrichment of the global ocean due to expansion of land ice during the LGM [*Schrag et al.*, 1996]. $\Delta\delta^{18}O_{LGM-LH}$ residuals after this correction were assumed to be exclusively attributable to a change in calcification temperature and were converted to SST anomalies using the low-light paleotemperature equation of *Bemis et al.* [1998], with a slope of −0.21‰/°C. This assumption neglects possible complications arising from (1) changes in seawater $\delta^{18}O$ composition related to regional precipitation/salinity variations, and (2) carbonate-ion effect on foraminiferal $\delta^{18}O$ [*Spero et al.*, 1997]. In two sites where SST has been independently estimated from Mg/Ca ratios, TR163-19 [*Lea et al.*, 2000] and V21-30 [*Koutavas et al.*, 2002], this assumption yields $\delta^{18}O$ results consistent with Mg/Ca and therefore appears justified. While this implicitly suggests that salinity and carbonate-ion effects were small, an alternate possibility may be that these two effects had opposing influences, partly canceling each other out during the LGM. For example, a plausible increase in salinity and seawater $\delta^{18}O$ due to ocean cooling and reduced precipitation (tending to enrich foraminiferal $\delta^{18}O$) may have been offset by increased surface ocean carbonate-ion concentration (tending to deplete foraminiferal $\delta^{18}O$). On the other hand an equatorward shift of the ITCZ such as we propose might have produced excess rainfall and therefore anomalously negative glacial $\delta^{18}O$ values. These effects remain unquantified and cannot be explicitly considered without independent estimates of regional salinity and carbonate-ion concentration reconstructions for the LGM. Nevertheless, in light of agreement between $\delta^{18}O$ and Mg/Ca cooling estimates in two of the 9 sites employed in this study we believe that the $\delta^{18}O$ approach used here yields reliable mean LGM SST anomalies relative to the LH.

[21] The pattern of LGM SST anomalies is shown in Figure 7b. Maximum cooling (2.4°–3.3°C) is indicated in the two northernmost sites, RC13-140 and TR163-19, and in the shore-proximal V19-27. By comparison, SST anomalies in the 6 sites south of 0.5°S range between 0° and 1.6°C. The factor of two or more larger cooling in the warmer waters north of the equator is also evident in Mg/Ca estimates from sites TR163-19 (2°15′N) and V21-30 (1°13′S), included in Figure 7b.

5.4. Glacial-Interglacial Changes in the EEP Cross-Equatorial Gradient

[22] We examine the evolution of the cross-equatorial gradient over the last 30 kyr as recorded by foraminiferal $\delta^{18}O$ in Figures 8a and 8b, where *G. ruber* and *G. sacculifer* $\delta^{18}O$ profiles respectively, from all cores, are plotted on a common scale. To facilitate comparison these sites are separated in two groups: a "southern" group consisting of V21-29, V21-30, RC8-102, RC11-238, V19-28, and V21-40 (displayed in blue tones), and a "northern" group consisting of RC13-140, TR163-19, and V19-27 (displayed in red-yellow tones). The southern cores give mean LH $\delta^{18}O$ values of ~−1.6‰ for *G. ruber* and ~−1.4‰ for *G. sacculifer*. These values are close to expectation as all southern sites are positioned near the -1.6 ± 0.1‰ predicted calcite $\delta^{18}O$ contour (Figures 1i and 7a). In the northern cores, LH $\delta^{18}O$ values range between −2.0‰ and −2.6‰ for *G. ruber*, (Figure 8a) and closer to −2.0‰ for *G. sacculifer* (Figure 8b). These values are again consistent with a predicted calcite $\delta^{18}O$ range of −2.0‰ to −2.5‰ for the northern sites, due to calcification in the warmer and fresher waters further north (Figures 1i and 7a). Both species therefore clearly record a mean north-south LH $\delta^{18}O$ gradient of 0.6–0.7‰, in accord with a predicted mean gradient of ~0.7‰ in the calcite $\delta^{18}O$ field, due to the modern hydrographic front.

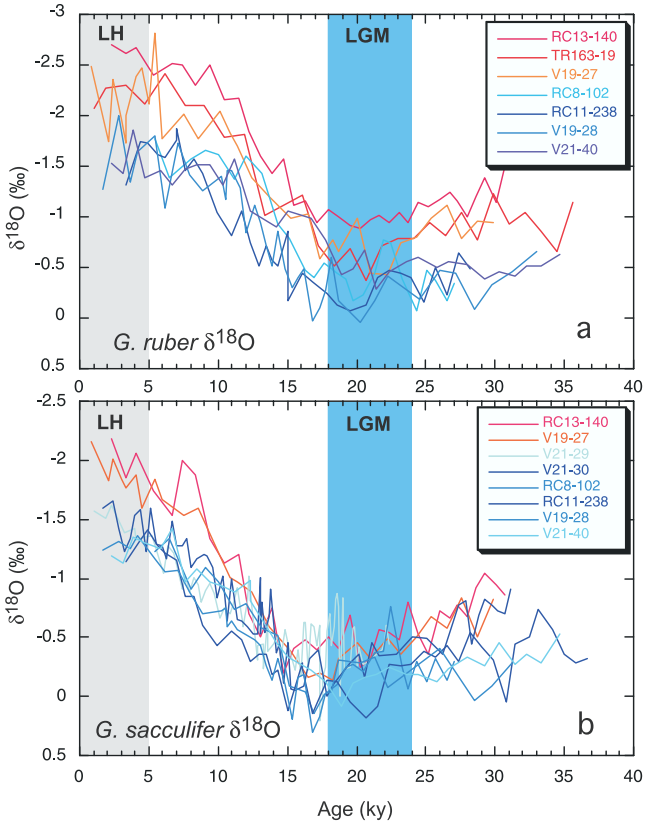

Figure 8. Composite of (a) *G. ruber* and (b) *G. sacculifer* $\delta^{18}O$ records from all EEP sites versus age. Records from the center of the cold tongue (1°–2°S) or further south are displayed in blue shades. Records from sites further north are displayed in red-yellow shades. Note that for each species the profiles from the northern cores (red-yellow) converge toward their southern counterparts (blue) during the LGM but begin to diverge at ~12 ky BP, and continue to do so through the Holocene.

[23] When plotted together (Figures 8a and 8b) both northern and southern groups display internally consistent downcore variation patterns: southern $\delta^{18}O$ records track one another closely with no evidence for systematic offsets among sites through the last 30 kyr. Similarly northern cores do not show systematic downcore offsets among sites for either species. However, comparison of the northern versus the southern sites clearly shows a larger north-south $\delta^{18}O$ contrast during the Holocene than in previous times including the LGM. This indicates that the modern (Holocene) meridional $\delta^{18}O$ gradient of 0.6–0.7‰ was reduced in glacial times, reaching modern values around 10–12 kyr BP. To obtain a first-order quantitative estimate of the change in gradient strength from the LGM to the LH we averaged northern group and southern group data from each species during these periods, and calculated the difference. The mean $\delta^{18}O$ gradient recorded by *G. sacculifer* was reduced from 0.56‰ in the LH to 0.21‰ in the LGM. Similarly, *G. ruber* shows a reduction in gradient from 0.70‰ in the LH to 0.37‰ in the LGM. These differences imply a mean LGM gradient reduction by 0.34‰ (48–62% of its LH value) which, if solely due to SST, corresponds to a reduction in the cross-equatorial SST gradient (between ~2°S and 3°N) by ~1.6°C. While salinity may have contributed to the observed $\delta^{18}O$ gradient reduction, modern hydrographic data show that the gradient is dominated by temperature, as is its seasonal (and interannual) modulation (Figure 1). Furthermore, comparison of the Mg/Ca SST records from TR163-19 and V21-30 (Figure 9) provides independent confirmation for an approximate doubling of the SST gradient between the two sites from the LGM to the Holocene.

[24] An alternative interpretation of the apparent weakening of the LGM cross-equatorial front as manifested in the $\delta^{18}O$ and Mg/Ca data may be that the front simply moved in position (for example if increased upwelling had caused the equatorial cold tongue to expand northward) while maintaining its intensity. In the modern climate extremely large changes in upwelling and hydrographic structure occur both seasonally and interannually, during which the SST front can vary from <1°C (e.g., during the peak of the 1997–98 El Niño) up to 8°C (e.g., during the 1988 La Niña). Despite such extreme variability the front is not observed to move latitudinally but remains fixed between 1°S and 5°N. This pattern is well documented in analysis of long data sets and appears to be an essential characteristic of both the seasonal and interannual upwelling pulses in the EEP [*Deser and Wallace*, 1990]. The underlying reason is that maximum divergence, which defines the coldest edge of the front is located precisely at the equator. For this reason we find it unlikely that the LGM front had moved with respect to the studied sites.

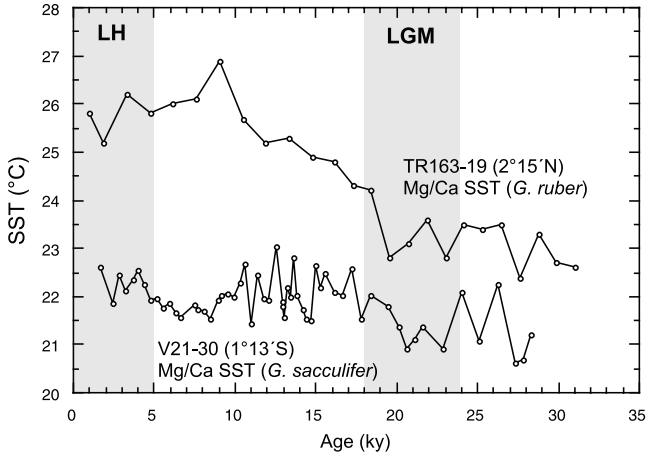

Figure 9. Comparison of Mg/Ca SST reconstructions from cores TR163-19 (2°15′N) [*Lea et al.*, 2000; *Spero and Lea*, 2002] and V21-30 (1°13′S) [*Koutavas et al.*, 2002]. The two cores span a latitudinal transect of 3.5° and a gradient in annual mean SST of 2.5°C, with seasonal extremes of 1° to 4°C. It is evident that the SST contrast between the two sites during the LGM was reduced to approximately half its Holocene value. Maximum gradient strength is indicated during the early to middle Holocene, 5–10 kyr BP. These data, based on a temperature proxy independent of $\delta^{18}O$, are consistent with the glacial-interglacial increase in cross-equatorial gradient we have inferred from $\delta^{18}O$ (Figure 8) and support the intensification of the cold tongue-ITCZ complex from the LGM to the Holocene.

6. Discussion

6.1. Factors Controlling the Cold Tongue-ITCZ Complex in the Modern Climate

[25] Our results indicate that the cross-equatorial front of the eastern tropical Pacific marking the transition from the cold tongue in the south to the ITCZ in the north was less intense in glacial times. In seeking to explain this result we first consider the mechanisms that maintain the cold tongue-ITCZ complex and associated front in the modern climate. This front is a prominent oceanographic feature and an integral part of the asymmetry in SST distribution about the equator, which manifests itself as a year-round presence of the warmest waters and the overlying ITCZ in the Northern Hemisphere. The origin of this asymmetry is thought to be ultimately related to the hemispheric land ratio and the continental geometry, in particular the slope of the western coast of the Americas with respect to the meridians, which causes offshore cooling by upwelling-favorable winds to be a more efficient process in the southern compared to the northern tropics [*Philander et al.*, 1996]. However, ocean-atmosphere interactions are instrumental in further amplifying this asymmetry. *Philander et al.* [1996] discuss four positive feedbacks that help accomplish this: (1) latent heat release causing enhancement of the rising motion in the convective region, which in turn helps intensify surface wind flow into the ITCZ; (2) a northward pressure-gradient force caused by the SST gradient which further reinforces the winds [*Lindzen and Nigam*, 1987]; (3) evaporative cooling in the cold tongue due to the strong wind flow over it; and (4), perhaps most critically, enhancement of surface cooling by stratus clouds forming over the cold waters south of the equator.

[26] The efficiency of these feedbacks varies seasonally as the insolation maximum crosses the equator. The seasonal insolation cycle attempts to restore symmetry about the equator by "pulling" the ITCZ southward during

austral summer. In the absence of land asymmetries the solar forcing should in theory cause a Southern Hemisphere summer ITCZ to develop, producing an annual mean climatology characterized by a double or split ITCZ [*Xie*, 1996]. This, however, is inhibited by the symmetry-breaking land forcing, which maintains a permanent Northern Hemisphere ITCZ, even as its latitudinal position migrates seasonally. *Mitchell and Wallace* [1992] examined in detail the seasonal evolution of the cold tongue-ITCZ in relation to convection strength, zonal and meridional wind stress, SST, and cloudiness. Their analysis links the annual appearance and intensification of the cold tongue with the onset of the northern summer monsoon, which strengthens the northward cross-equatorial winds during boreal spring and summer. Increased northward flow induces upwelling and surface cooling south of the equator. In turn, this cooling enhances the meridional and zonal pressure-gradient forces, further intensifying meridional and zonal wind flow, both of which promote upwelling and sustain the cold tongue. In the process the ITCZ attains its northernmost position. Stratus clouds forming south of the equator further enhance surface cooling by increasing the albedo, and appear to be instrumental in maintaining the cold tongue during its mature phase. In the presence of these positive feedbacks the cold tongue can be self-sustaining. According to *Mitchell and Wallace* [1992] its demise in boreal fall is linked to a perturbation of the wind field caused by the onset of the southern summer monsoon (October–November) when convection over land migrates to the Southern Hemisphere. The northward cross-equatorial flow in the EEP weakens causing the cold tongue to contract and permitting the oceanic front to relax and the ITCZ to move southward. Nevertheless, as noted, formation of an oceanic ITCZ in the Southern Hemisphere is inhibited. Contributing factors may include orographic blocking by the Andes and preconditioning of the ocean surface with cool SSTs, both of which are unfavorable to westward expansion of convection over the ocean, as occurs in the northern tropics.

[27] The relative role of the meridional and zonal wind components in driving upwelling and maintaining the cold tongue-ITCZ front is not entirely understood. *Mitchell and Wallace* [1992] found that cold-tongue SST is more highly correlated with meridional than zonal wind stress. A uniform northward meridional wind flow in the easternmost tropical Pacific has been shown in modeling studies to induce upwelling south of the equator, partly explaining why the cold tongue is centered south of the equator [*Cane*, 1979; *Philander and Pacanowski*, 1981]. Yet, satellite observations show that the wind field is far from uniform and is locally modified through the influence of SST on the vertical stability of the atmospheric boundary layer [*Chelton et al.*, 2001]. Over the coldest waters of the equatorial cold tongue the winds are up to four-fold weaker than to the south and north, apparently due to stabilization of the boundary layer by the cold SSTs. Increased stability inhibits downward mixing of northward momentum from the stronger winds aloft, decelerating the surface circulation [*Wallace et al.*, 1989; *Chelton et al.*, 2001]. Observed interactions between SST and the meridional and zonal wind component suggest that both play important roles for coupled air-sea dynamics in this region. Inadequate representations of the wind field in coupled GCMs in combination with poorly parameterized clouds invariably lead to serious deficiencies in reproducing the modern climatologic structure, producing SSTs that are insufficiently cool south of the equator, a cold tongue that is too narrow and extends too far west, and a spurious Southern Hemisphere ITCZ with unrealistically strong convection south of the equator [*Mechoso et al.*, 1995]. These inadequacies are likely to be important and must be considered when evaluating the ability of coupled GCMs to simulate the dynamical response of the equatorial Pacific in LGM experiments.

6.2. Factors Responsible for a Weaker Cold Tongue-ITCZ Complex During the LGM

[28] Given that cold tongue-ITCZ dynamics are instrumental in maintaining the equatorial SST asymmetry and possibly its westward propagation over the entire span of the tropical Pacific [*Mitchell and Wallace*, 1992], it is of fundamental interest to examine how the mean climatologic state had changed under LGM boundary conditions. Modeling studies bearing on this issue are divergent [e.g., *Bush and Philander*, 1999; *Shin et al.*, 2003], and may be biased by the endemic model limitations outlined above. Our data show that the oceanic front separating the cold tongue and ITCZ was relaxed in glacial times compared to the Holocene. This indicates that the asymmetry about the equator, though still present, was reduced. What could have caused this change? An obvious candidate is orbital forcing through its effect on the relative strength of the northern versus the southern summer monsoon. Northern summer (July) insolation was at a minimum during the LGM, whereas southern summer (January) insolation was at a maximum. A weak northern summer monsoon would not favor the annual development and intensification of the cold tongue, while the onset of a strong southern summer monsoon would promote its seasonal demise. Insofar as monsoon circulation is key in initiating convection alternately in each hemisphere, LGM insolation ought to have a symmetry-restoring influence. An overall weakening of the southeasterly wind flow over the cold tongue and across the equator, with consequent southward shift of the ITCZ and attenuation of the front is therefore a plausible consequence of LGM insolation forcing. Northern (southern) summer insolation increased (decreased) over the deglaciation, attaining a maximum (minimum) between 12-6 kyr BP. The resulting strengthening of the northern and weakening of the southern summer monsoon [e.g., *Kutzbach and Guetter*, 1986] would tend to reinforce the equatorial asymmetry in the early to-middle Holocene causing a pronounced northern ITCZ bias, well-developed cold tongue, and sharp front, consistent with our observations.

[29] We note, however, that orbitally induced monsoon dynamics cannot explain a weaker cold tongue-ITCZ front in the LGM compared to present because LGM and LH orbital forcing were similar. Other factors must have been important. One candidate is the ENSO system. El Niño suppresses upwelling in the cold tongue and shifts convection toward the equator. El Niño-like SST distribution

has been proposed as the prevailing pattern in the LGM [*Koutavas et al.*, 2002] although this may have been as much a consequence as a cause of a more symmetric SST field about the equator. Further, it is unclear as to how such a change in the time-mean background state was related to the frequency, amplitude or duration of individual warm or cold ENSO episodes.

[30] The presence of extensive land ice cover during the LGM deserves serious consideration as a key player in forcing an equatorward shift of the ITCZ. Such a shift could be accomplished through increased northern trades in the presence of permanent Northern Hemisphere ice sheets, and has been persuasively modeled in the Atlantic basin [*Chiang et al.*, 2003]. A parallel response in the Pacific, while plausible, remains to be demonstrated unequivocally, and is likely to require model advances in simulating the present-day climatology of that basin more accurately.

[31] Another important factor may have been a change in atmospheric water vapor content. The role of water vapor in fueling convection is two-fold: (1) through the release of latent heat as it condenses to form clouds, and (2) through greenhouse trapping of longwave radiation emitted from earth's surface [*Seager et al.*, 2000]. A postulated decrease in atmospheric humidity during the LGM [*Broecker*, 1997] may have been a potent way to inhibit rising motions in convective regions, thereby necessitating a decrease in low-level convergence compensating convective updraft. Reduced cross-equatorial low level winds in the EEP are consistent with a reduction in LGM Hadley circulation, particularly of the Southern Hemisphere cell, which is consistent with evidence that the glacial tropics were drier while the subtropics were wetter [*Thompson et al.*, 1998; *Rind*, 1998]. Reduced meridional winds due to weaker Hadley cell would have inhibited positive feedbacks due to upwelling and evaporative cooling in the cold tongue.

[32] Given the key role of low-level stratus clouds in the establishment and maintenance of the cold tongue in the modern climate [*Mitchell and Wallace*, 1992; *Philander et al.*, 1996; *Ma et al.*, 1996], the most effective mechanism for weakening the cold tongue-ITCZ complex in glacial times may have been by a reduction in low clouds over the upwelling region. The radiative forcing of low clouds is estimated at 1 W m^{-2} per percent change in cloud amount [*Klein and Hartmann*, 1993]. This compares, for example, with a forcing of 4 W m^{-2} for doubling of atmospheric CO_2. It follows that even a small change in stratus cloud cover can have a strong radiative impact at the surface and hence on SST over regions where stratus clouds form. Indeed, stratus clouds show strong negative correlation with underlying SST in modern observations [*Klein and Hartmann*, 1993; *Oreopoulos and Davies*, 1993]. Modeling studies suggest that low-level stratus clouds are in fact a negative climate feedback [*Miller*, 1997; *Seager et al.*, 2000], tending to increase in a warmer climate. Low clouds increase with increased static stability of the lower troposphere (defined as the difference in potential temperature between a level above the temperature inversion that caps the boundary layer, and the surface) [*Klein and Hartmann*, 1993]. While the surface temperature is coupled to the underlying SST, the temperature above the inversion is horizontally uniform and depends on surface conditions in convecting regions [*Miller*, 1997]. Using a simple model *Miller* [1997] showed that doubled CO_2 forcing increases the lower tropospheric static stability and promotes increased low clouds, due to a disproportionate increase of the temperature above the inversion compared to SST. The latter results in part from an increase in SST and moist convection in the model warm pool. In glacial times SSTs in convecting regions were reduced by ~3°C [*Lea et al.*, 2000; *Stott et al.*, 2002; *Visser et al.*, 2003] and therefore moist convection is likely to have been weaker. We infer that a decrease in low-level static stability of the glacial tropical atmosphere with attendant decrease in low cloud cover over the equatorial cold tongue and subtropical stratus regions is plausible, if not likely. We suggest that this may have been an effective cold-tongue limiting mechanism in the glacial EEP.

[33] The overall climatic response implied by our data for the Pacific, namely a southward shift of the ITCZ, weakening of the meridional front and contraction of the cold tongue is generally consistent with analogous climatic responses in the Atlantic basin where compelling evidence exists for a more southerly mean ITCZ latitude during glacial and stadial intervals [*Peterson et al.*, 2000; *Vink et al.*, 2001, *Arz et al.*, 1998]. Moreover, a recent GCM simulation using the NCAR CCSM coupled model [*Shin et al.*, 2003] is in general agreement with our results, showing mean LGM cooling of the EEP by 1°C and precipitation anomalies consistent with a southward shift of the tropical rainfall belt (although the model's tendency to produce a double ITCZ in the control run requires caution in interpreting its precipitation response). In this context we suggest that our proposed climatic response in the EEP is not only a plausible physical adjustment of the regional circulation to glacial boundary conditions, but also quite possibly part of a larger-scale fundamental tropical process involving coherent circum-global ITCZ dynamics across ocean basins.

7. Comparison With Previous Studies

[34] Several recent studies have employed reformulated faunal methods to estimate glacial cooling in the EEP [*Mix et al.*, 1999; *Feldberg and Mix*, 2002; *Trend-Staid and Prell*, 2002; *Feldberg and Mix*, 2003; *Martínez et al.*, 2003]. These methods typically indicate a strong glacial SST response with near-equatorial cooling in the range of 4°–8°C, far greater than suggested by our $\delta^{18}O$ data. A primary concern with these methods is the effect of seafloor dissolution in altering the faunal assemblages after deposition. Dissolution in the EEP is a severe problem below ~2800 m, although this depth shoals dramatically eastward toward the continental margin as increasing organic rain rates drive higher pore water dissolution. Many of the sites utilized by the recent faunal census studies exceed this depth making a marked dissolution influence unavoidable (inspection of some of these sites has led us to reject them for isotopic study because of evident dissolution problems, e.g., sites V19-29, V19-30, V21-33, RC13-110, RC13-113, RC13-114), although it is not clear that this is the ultimate source of the discrepancy with our isotopic data. Additional

factors may be at play, as for example an apparent pycnocline bias in the transfer functions of *Mix et al.* [1999] and *Feldberg and Mix* [2002], which leads to underestimation of SSTs as upper ocean density stratification increases. Finally, we note that the large SST anomalies recovered by the faunal methods are driven in large part by a pronounced glacial spike in *Globorotalia inflata* recognized in early studies [e.g., *Luz*, 1973], which appears to be restricted to the path of the south equatorial current south of 2°S and east of 110°W [*Martínez et al.*, 2003], the region where faunal methods display their largest SST anomalies [*Mix et al.*, 1999; *Trend-Staid and Prell*, 2002]. *G. inflata* is a transitional species with a sub-thermocline habitat which is presently associated with the eastern boundary Peru-Chile Current (PCC). Its glacial expansion into the equatorial cold tongue may be related to increased advection rates of PCC waters [*Feldberg and Mix*, 2003], increased proliferation of *G. inflata* in the glacial PCC without a necessary increase in advective transport, or perhaps the removal of an environmental barrier such as oxygen limitation, as originally proposed by *Luz* [1973], or even to altered nutrient properties of the equatorial undercurrent originating in the Subantarctic [*Loubere*, 2000]. We suspect that downcore variations in the abundance of this subsurface species may be imparting an excessive cold bias in the faunal LGM temperature estimates, which may not be directly related to surface hydrography or the intensity of equatorial upwelling. Our study adds a further layer of complexity to the interpretation of these faunal methods but it also provides needed constraints for ultimately understanding and resolving the existing dichotomy between faunal and geochemical indices in the EEP.

[35] It has been argued that the LGM descent of tropical snow lines by ~800 m (corrected for sea level) implies substantial high-altitude cooling, which, barring an increase in lapse rates, necessitates a drop in tropical SST by 4°–5°C [*Rind and Peteet*, 1985]. In addition, the $\delta^{18}O$ composition of ice from the Huascaran, Peru ice core has been interpreted to impose a similar requirement [*Thompson et al.*, 1995]. Our estimate for mean cooling of the equatorial cold tongue by ~1.5°C poses a question of consistency with the snow line and ice core evidence from the tropical Andes. *Pierrehumbert* [1999] addressed the ice core $\delta^{18}O$ evidence showing that it is in fact consistent with a ~3°C drop in mean tropical SST. *Betts and Ridgway* [1992] further showed, using a radiative-convective model, that a snow line lowering of 800 m is compatible with mean tropical cooling of 2°C, or as little as 1.4°C if a 30% reduction in surface wind speed is assumed. Weaker winds in the EEP during the LGM appear plausible given our finding of reduced SST gradients. Using a similar model *Greene et al.* [2002], estimated that a mean SST reduction of 2.8°C in convecting regions of the tropics is both necessary and sufficient for explaining the observed LGM snow line depressions. Smaller cooling requirements are imposed in the case of reduced winds, and larger in the case of reduced precipitation. We note that these model estimates reflect average tropical SSTs and therefore allow for spatially nonuniform cooling patterns. In this light we do not view our results as being in conflict with climate records from the high Andes.

8. Summary and Conclusions

[36] We have presented new downcore planktonic $\delta^{18}O$ records from the EEP and used them to (1) constrain the magnitude of glacial cooling in the equatorial cold tongue, and (2) reconstruct the glacial-interglacial pattern of variation in the cross-equatorial cold tongue-ITCZ front. Cold-tongue SST during the LGM is found to have experienced a modest decrease of 1.5 ± 0.5°C, compared to decreases of 2.5°–3°C in sites further north. Comparison of downcore $\delta^{18}O$ variations during the last 30 kyr between the northernmost and southernmost sites similarly indicates that the cold tongue-ITCZ hydrographic front doubled in intensity from the LGM to the Holocene.

[37] We interpret this result as part of a large-scale dynamical response of the coupled tropical Pacific ocean-atmosphere, which includes the following features: (1) reduction in the dominance of cold-tongue upwelling in the EEP, (2) relaxation of low-latitude zonal and meridional SST gradients, (3) substantial (~3°C) cooling in oceanic regions of deep convection such as the warm pool and ITCZ with attendant reduction in convective updraft, (4) overall weakening of the Walker overturning circulation with a tendency for weaker southeast trades in the EEP, (5) equatorward displacement of the Pacific ITCZ, and (6) reduction of low cloud cover over upwelling regions. While our reconstruction offers direct support for many of these features, further investigation is required to confirm and augment our observations. If these climate features were indeed prevalent in the glacial tropical Pacific, their impact on global climate may have been of overwhelming importance. Ongoing paleoclimate reconstructions in conjunction with model refinements and data-model convergence are essential prerequisites for exploring this question in all its dimensions with sufficient confidence.

[38] **Acknowledgments.** We thank Mark A. Cane for a critical reading of the manuscript, John C. H. Chiang for in-depth discussions, and Linda Baker, Pat Malone, Grace Kim and Greta Fails for technical assistance. We acknowledge the thoughtful reviews by D. W. Lea and L. Stott which benefited the manuscript substantially. This work was supported by a National Science Foundation (NSF) CAREER award and a grants/cooperative agreement from the National Oceanic and Atmospheric Administration (NOAA). The views expressed herein are those of the authors and do not necessarily reflect those of NOAA or any of its subagencies. Sample material used in this project provided by the Lamont-Doherty Earth Observatory Deep-Sea Sample Repository. Support for the collection and curating facilities of the core collection is provided by NSF through grant OCE00-02380 and the Office of Naval Research through grant N00014-02-1-0073.

References

Andreasen, D. J., and A. C. Ravelo, Tropical Pacific Ocean thermocline depth reconstructions for the last glacial maximum, *Paleoceanography*, *12*, 395–413, 1997.

Andreasen, D. H., A. C. Ravelo, and A. J. Broccoli, Remote forcing at the Last Glacial Maximum in the tropical Pacific Ocean, *J. Geophys. Res.*, *106*, 879–897, 2001.

Andrus, C. F. T., D. E. Crowe, D. H. Sandweiss, E. J. Reitz, and C. S. Romanek, Otolith $\delta^{18}O$ record of mid-Holocene sea surface temperatures in Peru, *Science*, *295*, 1508–1511, 2002.

Arz, H. W., J. Pätzold, and G. Wefer, Correlated millennial-scale changes in surface hydrography and terrigenous sediment yield inferred from last-glacial marine deposits off northeastern Brazil, *Quat. Res.*, *50*, 157–166, 1998.

Bé, A. W. H., Gametogenic calcification in a spinose planktonic foraminifer, *Globigerinoides sacculifer* (Brady), *Mar. Micropaleontol.*, *5*, 283–310, 1980.

Bé, A. W. H., D. S. and Tolderlund, Distribution and ecology of living planktonic foraminifera in surface waters of the Atlantic and Indian Oceans, in *The Micropaleontology of Oceans*, edited by B. M. Funnell and W. R. Riedel, pp. 105–149, Cambridge Univ. Press, New York, 1971.

Bé, A. W. H., H. J. Spero, and O. R. Anderson, Effects of symbiont elimination and reinfection on the life processes of the planktonic foraminifer *Globigerinoides sacculifer*, *Mar. Biol.*, *70*, 73–86, 1982.

Beaufort, L., T. de Garidel-Thoron, A. C. Mix, and N. G. Pisias, ENSO-like forcing on oceanic primary production during the late Pleistocene, *Science*, *293*, 2440–2444, 2001.

Bemis, B. E., H. J. Spero, J. Bijma, and D. W. Lea, Reevaluation of the oxygen isotopic composition of planktonic foraminifera: Experimental results and revised paleotemperature equations, *Paleoceanography*, *13*, 150–160, 1998.

Betts, A. K., and W. Ridgway, Tropical boundary layer equilibrium in the last ice age, *J. Geophys. Res.*, *97*, 2529–2534, 1992.

Bijma, J., W. W. Faber Jr., and C. Hemleben, Temperature and salinity limits for growth and survival of some planktonic foraminifers in laboratory cultures, *J. Foraminiferal Res.*, *20*, 95–116, 1990.

Broecker, W. S., Oxygen isotope constraints on surface ocean temperatures, *Quat. Res.*, *26*, 121–134, 1986.

Broecker, W. S., Mountain glaciers: Recorders of atmospheric water vapor content?, *Global Biogeochem. Cycles*, *11*, 589–597, 1997.

Bush, A. B. G., and S. G. H. Philander, The climate of the last glacial maximum: Results from a coupled atmosphere-ocean general circulation model, *J. Geophys. Res.*, *104*, 24,509–24,525, 1999.

Cane, M., The response of an equatorial ocean to simple wind patterns: II. Numerical results, *J. Mar. Res*, *37*, 253–299, 1979.

Cane, M., A role for the tropical Pacific, *Science*, *282*, 59–61, 1998.

Cane, M., and A. C. Clement, A role for the tropical Pacific coupled ocean-atmosphere system on Milankovitch and millennial timescales: 2. Global impacts, in *Mechanisms of Global Climate Change at Millennial Timescales*, *Geophys. Monogr. Ser.*, vol. 112, edited by P. U. Clark, R. S. Webb, and L. D. Keigwin, pp. 373–383, AGU, Washington, D. C., 1999.

Chavez, F. P., P. G. Strutton, G. E. Friederich, R. A. Feely, G. C. Feldman, D. G. Foley, and M. J. McPhaden, Biological and chemical response of the equatorial Pacific Ocean to the 1997–98 El Niño, *Science*, *286*, 2126–2131, 1999.

Chelton, D. B., S. K. Esbensen, M. G. Schlax, N. Thum, M. H. Freilich, F. J. Wentz, C. L. Gentemann, M. J. McPhaden, and P. S. Schopf, Observations of coupling between surface wind stress and sea surface temperature in the eastern tropical Pacific, *J. Clim.*, *14*, 1479–1498, 2001.

Chiang, J. C. H., M. Biasutti, and D. S. Battisti, Sensitivity of the Atlantic Intertropical Convergence Zone to Last Glacial Maximum boundary conditions, *Paleoceanography*, *18*, doi:10.1029/2003PA000916, in press, 2003.

Clement, A. C., and M. A. Cane, A role for the tropical Pacific coupled ocean-atmosphere system on Milankovitch and millennial timescales: 2. A modeling study of tropical Pacific variability, in *Mechanisms of Global Climate Change at Millennial Timescales*, *Geophys. Monogr. Ser.*, vol. 112, edited by P. U. Clark, R. S. Webb, and L. D. Keigwin, pp. 363–371, AGU, Washington, D. C., 1999.

Clement, A. C., R. Seager, and M. A. Cane, Orbital controls on the El Niño/Southern Oscillation and the tropical climate, *Paleoceanography*, *14*, 441–456, 1999.

CLIMAP project members, *Seasonal Reconstruction of the Earth's Surface at the Last Glacial Maximum*, *Map and Chart Ser.*, vol. 36, Geol. Soc. of Am., Boulder, Colo., 1981.

Coale, K. H., et al., A massive phytoplankton bloom induced by an ecosystem-scale iron fertilization experiment in the equatorial Pacific Ocean, *Nature*, *383*, 495–501, 1996.

Codron, F., Sensitivity of the tropical Pacific to a change of orbital forcing in two versions of a coupled GCM, *Clim. Dyn.*, *17*, 187–203, 2001.

Crowley, T. J., CLIMAP SSTs re-revisited, *Clim. Dyn.*, *16*, 241–255, 2000.

Curry, W. B., R. C. Thunell, and S. Honjo, Seasonal changes in the isotopic composition of planktonic foraminifera collected in Panama Basin sediment traps, *Earth Planet. Sci. Lett.*, *64*, 33–43, 1983.

Deser, C., and J. M. Wallace, Large-scale atmospheric circulation features of warm and cold episodes in the tropical Pacific, *J. Clim.*, *3*, 1254–1281, 1990.

Dugdale, R., and F. Wilkerson, Silicate regulation of new production in the equatorial Pacific upwelling, *Nature*, *391*, 270–273, 1998.

Fairbanks, R. G., M. Sverdlove, R. Free, P. H. Wiebe, and A. W. H. Bé, Vertical distribution and isotopic fractionation of living planktonic foraminifera from the Panama Basin, *Nature*, *298*, 841–844, 1982.

Farrell, J. W., D. W. Murray, V. S. McKenna, and A. C. Ravelo, Upper ocean temperature and nutrient contrasts inferred from Pleistocene planktonic foraminifer $\delta^{18}O$ and $\delta^{13}C$ in the eastern equatorial Pacific, *Proc. Ocean Drill. Prog.*, *138*, 289–319, 1995.

Faul, K. L., A. C. Ravelo, and M. L. Delaney, Reconstructions of upwelling, productivity, and photic zone depth in the eastern equatorial Pacific Ocean using planktonic foraminiferal stable isotopes and abundances, *J. Foraminiferal Res.*, *30*, 110–125, 2000.

Feldberg, M. J., and A. C. Mix, Sea-surface temperature estimates in the southeast Pacific based on planktonic foraminiferal species: Modern calibration and Last Glacial Maximum, *Mar. Micropaleontol.*, *44*, 1–29, 2002.

Feldberg, M. J., and A. C. Mix, Planktonic foraminifera, sea surface temperatures, and mechanisms of oceanic change in the Peru and south equatorial currents, 0–150 ka BP, *Paleoceanography*, *18*(1), 1016, doi:10.1029/2001PA000740, 2003.

Greene, A. M., R. Seager, and W. S. Broecker, Tropical snowline depression at the Last Glacial Maximum: Comparison with proxy records using a single-cell tropical climate model, *J. Geophys. Res.*, *107*(D8), 4061, doi:10.1029/2001JD000670, 2002.

Halpert, M. S., and C. F. Ropelewski, Surface temperature patterns associated with the Southern Oscillation, *J. Clim.*, *5*, 577–593, 1992.

Hendy, E. J., M. K. Gagan, C. A. Alibert, M. T. McCulloch, J. M. Lough, and P. J. Isdale, Abrupt decrease in tropical Pacific sea surface salinity at end of little ice age, *Science*, *295*, 1511–1514, 2002.

Kitagawa, H., and J. van der Plicht, A 40,000-year varve chronology from Lake Suigetsu, Japan: Extension of the ^{14}C calibration curve, *Radiocarbon*, *40*, 505–515, 1998.

Klein, S. A., and D. L. Hartmann, The seasonal cycle of low stratiform clouds, *J. Clim.*, *6*, 1587–1606, 1993.

Koutavas, A., J. Lynch-Stieglitz, T. M. Marchitto Jr., and J. P. Sachs, El Niño-like pattern in ice age tropical Pacific sea surface temperature, *Science*, *297*, 226–230, 2002.

Kutzbach, J. E., and P. J. Guetter, The influence of changing orbital parameters and surface boundary conditions on climate simulations for the past 18,000 years, *J. Atmos. Sci.*, *43*, 1726–1759, 1986.

Lea, D. W., D. K. Pak, and H. J. Spero, Climate impact of late Quaternary equatorial Pacific sea surface temperature variations, *Science*, *289*, 1719–1724, 2000.

Levitus, S., and T. P. Boyer, *World Ocean Atlas 1994*, vol. 4, *Temperature*, *NOAA Atlas NESDIS 4*, U.S. Dept. of Commerce, Washington, D. C., 1994.

Levitus, S., R. Burgett, and T. P. Boyer, *World Ocean Atlas 1994*, vol. 3, *Salinity*, *NOAA Atlas NESDIS 3*, U.S. Dept. of Commerce, Washington, D. C., 1994.

Li, T., and S. G. H. Philander, On the annual cycle of the eastern equatorial Pacific, *J. Clim.*, *9*, 2986–2998, 1996.

Lindzen, R. S., and S. Nigam, On the role of sea surface temperature gradients in forcing low-level winds and convergence in the tropics, *J. Atmos. Sci.*, *14*, 2418–2436, 1987.

Liu, Z., E. Brady, and J. Lynch-Stieglitz, Global ocean response to orbital forcing in the Holocene, *Paleoceanography*, *18*(2), 1041, doi:10.1029/2002PA000819, 2003.

Lohmann, G. P., A model for variation in the chemistry of planktonic foraminifera due to secondary calcification and selective dissolution, *Paleoceanography*, *10*, 445–457, 1995.

Loubere, P., Marine control of biological production in the eastern equatorial Pacific Ocean, *Nature*, *406*, 497–500, 2000.

Luz, B., Stratigraphic and paleoclimatic analysis of Late Pleistocene tropical southeast Pacific cores, *Quat. Res.*, *3*, 56–72, 1973.

Lyle, M., D. W. Murray, B. P. Finney, J. Dymond, J. M. Robbins, and K. Brooksforce, The record of late Pleistocene biogenic sedimentation in the eastern tropical Pacific Ocean, *Paleoceanography*, *3*, 39–59, 1988.

Lyle, M. W., F. G. Prahl, and M. A. Sparrow, Upwelling and productivity changes inferred from a temperature record in the central equatorial Pacific, *Nature*, *355*, 812–815, 1992.

Ma, C.-C., C. R. Mechoso, A. W. Robertson, and A. Arakawa, Peruvian stratus clouds and the tropical Pacific circulation: A coupled ocean-atmosphere GCM study, *J. Clim.*, *9*, 1635–1645, 1996.

Marcantonio, F., R. F. Anderson, S. Higgins, M. Stute, P. Schlosser, and P. Kubik, Sediment focusing in the central equatorial Pacific Ocean, *Paleoceanography*, *16*, 260–267, 2001.

Martínez, I., L. Keigwin, T. T. Barrows, Y. Yokoyama, and J. Southon, La Niña-like

conditions in the eastern equatorial Pacific and a stronger Choco jet in the northern Andes during the last glaciation, *Paleoceanography*, *18*(2), 1033, doi:10.1029/2002PA000877, 2003.

Mechoso, C. R., et al., The seasonal cycle over the tropical Pacific in coupled ocean-atmosphere general circulation models, *Mon. Weather Rev.*, *123*, 2825–2838, 1995.

Miller, R. L., Tropical thermostats and low cloud cover, *J. Clim.*, *10*, 409–440, 1997.

Mitchell, T. P., and J. M. Wallace, The annual cycle of equatorial convection and sea surface temperature, *J. Clim.*, *5*, 1140–1156, 1992.

Mix, A. C., A. E. Morey, N. G. Pisias, and S. W. Hostetler, Foraminiferal faunal estimates of paleotemperature: Circumventing the no-analog problem yields cool ice age tropics, *Paleoceanography*, *14*, 350–359, 1999.

Mix, A. C., E. Bard, and R. Schneider, Environmental processes of the ice age: Land, oceans, glaciers (EPILOG), *Quat. Sci. Rev.*, *20*, 627–657, 2001.

Murray, J. W., R. T. Barber, M. R. Roman, M. P. Bacon, and R. A. Feely, Physical and biological controls on carbon cycling in the equatorial Pacific, *Science*, *266*, 58–65, 1994.

Oreopoulos, L., and R. Davies, Statistical dependence of albedo and cloud cover on sea surface temperature for two tropical marine stratocumulus regions, *J. Clim.*, *6*, 2434–2447, 1993.

Pak, H., and J. R. V. Zaneveld, Equatorial front in the eastern Pacific Ocean, *J. Phys. Oceanogr.*, *4*, 570–578, 1974.

Patrick, A., and R. C. Thunell, Tropical sea surface temperatures and upper water column thermal structure during the last glacial maximum, *Paleoceanography*, *12*, 649–657, 1997.

Paytan, A., M. Kastner, and F. P. Chavez, Glacial to interglacial fluctuations in productivity in the equatorial Pacific as indicated by marine barite, *Science*, *274*, 1355–1357, 1996.

Pedersen, T. F., Increased productivity in the eastern equatorial Pacific during the Last Glacial Maximum (19,000 to 14,000 yr B. P.), *Geology*, *11*, 16–19, 1983.

Pedersen, T. F., B. Nielsen, and M. Pickering, Timing of late Quaternary productivity pulses in the Panama Basin and implications for atmospheric CO_2, *Paleoceanography*, *6*, 657–677, 1991.

Peterson, L. C., G. H. Haug, K. A. Hughen, and U. Röhl, Rapid changes in the hydrologic cycle of the tropical Atlantic during the last glacial, *Science*, *290*, 147–151, 2000.

Philander, S. G. H., and R. C. Pacanowski, The ocean response to cross-equatorial winds (with application to coastal upwelling in low latitudes), *Tellus*, *33*, 201–210, 1981.

Philander, S. G. H., D. Gu, D. Halpern, G. Lambert, N.-C. Lau, T. Li, and R. C. Pacanowski, Why the ITCZ is mostly north of the equator, *J. Clim.*, *9*, 2958–2972, 1996.

Pierrehumbert, R. T., Huascaran $\delta^{18}O$ as an indicator of tropical climate during the last glacial maximum, *Geophys. Res. Lett.*, *26*, 1345–1348, 1999.

Pierrehumbert, R. T., Climate change and the tropical Pacific: The sleeping dragon wakes, *Proc. Nat. Acad. Sci.*, *97*, 1355–1358, 2000.

Pisias, N. G., and A. C. Mix, Spatial and temporal oceanographic variability of the eastern equatorial Pacific during the late Pleistocene: Evidence from radiolaria microfossils, *Paleoceanography*, *12*, 381–393, 1997.

Ravelo, A. C., and N. J. Shackleton, Evidence for surface-water circulation changes at site 851 in the eastern tropical Pacific Ocean, *Proc. Ocean Drill. Program*, *138*, 503–514, 1995.

Rind, D., Latitudinal temperature gradients and climate change, *J. Geophys. Res.*, *103*, 5943–5971, 1998.

Rind, D., and D. Peteet, Terrestrial conditions at the Last Glacial Maximum and CLIMAP sea-surface temperature estimates: Are they consistent?, *Quat. Res.*, *24*, 1–22, 1985.

Rosenthal, Y., G. P. Lohmann, K. C. Lohmann, and R. M. Sherrell, Incorporation and preservation of Mg in *Globigerinoides sacculifer*: Implications for reconstructing the temperature and $^{18}O/^{16}O$ of seawater, *Paleoceanography*, *15*, 135–145, 2000.

Schrag, D. P., G. Hampt, and D. W. Murray, Pore fluid constraints on the temperature and oxygen isotopic composition of the glacial ocean, *Science*, *272*, 130–132, 1996.

Seager, R., A. C. Clement, and M. A. Cane, Glacial cooling in the tropics: Exploring the roles of tropospheric water vapor, surface wind speed, and boundary layer processes, *J. Atmos. Sci.*, *57*, 2144–2157, 2000.

Shackleton, N. J., The oxygen isotope stratigraphic record of the Late Pleistocene, *Philos. Trans. R. Soc. London B.*, *280*, 169–182, 1977.

Shin, S.-I., Z. Liu, B. Otto-Bliesner, E. C. Brady, J. E. Kutzbach, and S. P. Harrison, A simulation of the Last Glacial Maximum climate using the NCAR-CCSM, *Clim. Dyn.*, *20*, 127–151, 2003.

Soden, B. J., Variations in the tropical greenhouse effect during El Niño, *J. Clim.*, *10*, 1050–1055, 1997.

Spero, H. J., and D. W. Lea, The cause of carbon isotope minimum events on glacial terminations, *Science*, *296*, 522–525, 2002.

Spero, H. J., J. Bijma, D. W. Lea, and B. E. Bemis, Effect of seawater carbonate concentration on foraminiferal carbon and oxygen isotopes, *Nature*, *390*, 497–500, 1997.

Stott, L., C. Poulsen, S. Lund, and R. Thunell, Super ENSO and global climate oscillations at millennial time scales, *Science*, *297*, 222–226, 2002.

Stuiver, M., P. J. Reimer, E. Bard, J. W. Beck, G. S. Burr, K. A. Hughen, B. Kromer, G. McCormac, J. van der Plicht, and N. Spurk, INTCAL98 radiocarbon age calibration 24,000-0 cal BP, *Radiocarbon*, *40*, 1041–1083, 1998.

Thompson, L. G., E. Mosley-Thompson, M. E. Davis, P.-N. Lin, K. A. Henderson, J. Cole-Dai, J. F. Bolzan, and K.-B. Liu, Late glacial stage and Holocene tropical ice core records from Huascaran Peru, *Science*, *269*, 46–50, 1995.

Thompson, L. G., et al., A 25-000-year tropical climate history from Bolivian ice cores, *Science*, *282*, 1858–1864, 1998.

Thunell, R. C., and L. A. Reynolds, Sedimentation of planktonic foraminifera: Seasonal changes in species flux in the Panama Basin, *Micropaleontology*, *30*, 243–262, 1984.

Thunell, R. C., R. S. Keir, and S. Honjo, Calcite dissolution: An in situ study in the Panama basin, *Science*, *212*, 659–661, 1981.

Thunell, R. C., W. B. Curry, and S. Honjo, Seasonal variation in the flux of planktonic foraminifera: Time series sediment trap results from the Panama Basin, *Earth Planet. Sci. Lett.*, *64*, 44–55, 1983.

Trenberth, K. E., and J. W. Hurrell, Decadal atmosphere-ocean variations in the Pacific, *Clim. Dyn.*, *9*, 303–319, 1994.

Trenberth, K. E., G. W. Branstator, D. Karoly, A. Kumar, N.-C. Lau, and C. Ropelewski, Progress during TOGA in understanding and modeling global teleconnections associated with tropical sea surface temperatures, *J. Geophys. Res.*, *103*, 14,291–14,324, 1998.

Trend-Staid, M., and W. L. Prell, Sea surface temperature at the Last Glacial Maximum: A reconstruction using the modern analog technique, *Paleoceanography*, *17*(4), 1065, doi:10.1029/2000PA000506, 2002.

Urban, F. E., J. E. Cole, and J. T. Overpeck, Influence of mean climate change on climate variability from a 155-year tropical Pacific coral record, *Nature*, *407*, 989–993, 2000.

Vink, A., C. Rühlemann, K. A. F. Zonneveld, S. Mulitza, M. Hüls, and H. Willems, Shifts in the position of the north equatorial current and rapid productivity changes in the western tropical Atlantic during the last glacial, *Paleoceanography*, *16*, 1–12, 2001.

Visser, K., R. Thunell, and L. Stott, Magnitude and timing of temperature change in the Indo-Pacific warm pool during deglaciation, *Nature*, *421*, 152–155, 2003.

Wallace, J. M., T. P. Mitchell, and C. Deser, The influence of sea surface temperature on surface wind in the eastern equatorial Pacific: Seasonal and interannual variability, *J. Clim.*, *2*, 1492–1499, 1989.

Xie, S.-P., Effects of seasonal solar forcing on latitudinal asymmetry of the ITCZ, *J. Clim.*, *9*(11), 2945–2953, 1996.

Yin, J. H., and D. S. Battisti, The importance of tropical sea surface temperature patterns in simulations of the last glacial maximum climate, *J. Clim.*, *14*, 565–581, 2001.

A. Koutavas, Department of Earth, Atmospheric and Planetary Sciences, Massachusetts Institute of Technology, Cambridge, MA 02139, USA. (koutavas@mit.edu)

J. Lynch-Stieglitz, Lamont-Doherty Earth Observatory, Columbia University, Palisades, NY 10964, USA. (jean@ldeo.columbia.edu)